NANOSYSTEMS:
PHYSICS, CHEMISTRY, MATHEMATICS

Ulyanova E.S., Shalaeva E.V., et al. *Nanosystems: Phys. Chem. Math.*, 2022, **13** (4), 445–455.
http://nanojournal.ifmo.ru
DOI 10.17586/2220-8054-2022-13-4-445-455

Original article

Near-IR photoluminescence and structural properties of TiO_2 powders with nanocrystalline anatase/brookite matrix

Ekaterina S. Ulyanova[1,a], Elizaveta V. Shalaeva[1,b], Yuriy S. Ponosov[2,c], Olga A. Lipina[1,d], Alexey A. Markov[1,e]

[1]Institute of Solid State Chemistry of Ural Branch of the Russian Academy of Sciences, Ekaterinburg, Russia
[2]M. N. Mikheev Institute of Metal Physics of Ural Branch of the Russian Academy of Sciences, Ekaterinburg, Russia

[a]tsivileva.yekaterina@yandex.ru, [b]shalaeva@ihim.uran.ru, [c]ponosov@imp.uran.ru, [d]LipinaOlgaA@yandex.ru, [e]aamarkov1@yandex.ru

Corresponding author: Ekaterina S. Ulyanova, tsivileva.yekaterina@yandex.ru

PACS 81.07.-b, 78.30.j, 78.55.-m, 73.20.Hb

ABSTRACT The properties are studied for near-IR photoluminescence (PL) observed at 865 – 870 nm for precipitated TiO_2 powders having nanocrystalline anatase/brookite structure: the dependence of NIR PL on annealing in oxygen, on content and crystallinity quality of brookite, and on excitation energy (E_{ex}). NIR PL in bi-phase powders was found to demonstrate a behavior characteristic of NIR PL in brookite. NIR emission intensity grows with increasing brookite content and at annealing in oxygen, when oxygen vacancies content decreases and crystallinity quality of brookite improves. The results indicate that in the bi-phase powders, brookite contains deep-level defect traps which are regarded responsible for NIR-PL in brookite and are favorable for photocatalytic reactions. NIR emission is observed for the band ($E_{ex} \approx E_b$) and below band-gap green ($E_{ex} < E_b$) excitation. A mechanism underlying NIR-PL in brookite with green excitation is suggested to be similar to that for the red PL known for anatase at below band-gap excitation.

KEYWORDS anatase/brookite TiO_2, nano-powders, NIR-photoluminescence, structural properties, defect states

ACKNOWLEDGEMENTS The authors are grateful to Dr. I. V. Baklanova for measurements of IR-spectra. The research was carried out in accordance with the state assignment for ISSC UB RAS and financial support from ISSC UB RAS (theme AAAA-A19-119031890025-9). Yu. S. P. acknowledges financial support from Ministry of Science and Higher Education of the Russian Federation (theme "Electron" No. 122021000039-4).

FOR CITATION Ulyanova E.S., Shalaeva E.V., Ponosov Yu.S., Lipina O.A., Markov A.A. Near-IR photoluminescence and structural properties of TiO_2 powders with nanocrystalline anatase/brookite matrix. *Nanosystems: Phys. Chem. Math.*, 2022, **13** (4), 445–455.

1. Introduction

Until recently, major research attention has been dedicated to the creation of photoactive materials to be based on anatase and rutile polymorphs of titanium dioxide and on their combinations [1–3]. It is only over the last years that intensive studies have been under way, reporting one more low-temperature, metastable polymorph of titanium dioxide, namely, brookite and its combinations with anatase [4–11]. Brookite has an advantage that is perceived to be in having structural defects/electron traps with the energy depth greater than that of anatase and smaller than that of rutile, which favors a more effective process of separation of photogenerated electron-hole pairs and provides for a longer life of charge carriers [10]. According to some researchers, it is exactly the reason why brookite nanoparticles and nanocrystals have excellent photocatalytic properties [5, 10, 11]. Similarly to single-phase brookite samples, mixed anatase/brookite nanocrystalline matrices also have good photocatalytic characteristics in some redox reactions [12–14]. Such good properties are found to be demonstrated by bi-crystalline hydrothermally synthesized TiO_2 with coherent interfaces between nanoparticles of brookite and anatase [12], mixed anatase and brookite nanoparticles [13], as well as aggregated nanocrystalline powders with anatase/brookite structure synthesized using the wet precipitation method [14]. Besides, binary anatase/brookite matrix is of additional research interest, which is caused by good photocatalytic properties of the composites containing sulfides and obtained in-situ by the wet precipitation method [15].

Improved photocatalytic properties of bi-crystalline anatase/brookite TiO_2 are related, firstly, to the fact that brookite has a more negative conduction band which may induce electron transfer from brookite to anatase via coherent interface thus enhancing charge separation, and, secondly, to the intrinsic defects in brookite, which act as deep traps enhancing the

electron trapping [13]. HRTEM study does not reveal coherent boundaries anatase/brookite in the aggregated nano powders, unlike the bi-crystalline TiO_2 [14, 16]. In this regard, to find out the causes for improved photocatalytic properties and to further clarify the separation mechanisms of photogenerated carriers in the mixed nano powders, it appears necessary to have information on the defects that play the role of electron traps and are presented in the brookite component of such mixed matrices. It is also deemed important to determine the energy range (UV only or visible light) within which these defect states get excited.

Photoluminescence (or else fluorescence) is one of the major methods for characterizing the energy of radiative recombination of photogenerated carriers (electrons and holes) [17]. A photoluminescence energy spectrum provides information on the basic energy level of structural defects that play the role of charge carrier traps at certain excitation energy, which is to be selected close or slightly lower than the energy gap width. For nano-sized objects, photoluminescence demonstrates high sensitivity to defects in the near-the-surface layer and thus turns out to be quite useful for photocatalytic applications [18]. By now, a considerable body of research has been carried out on the photoluminescence (PL) for nanostructured single-phase anatase and PL mechanisms have been suggested that are associated with defects in anatase [19–26]. Photoluminescence in anatase is known to be observed in a wide range of the visible light spectrum from 400 nm up to nearly 700 nm. Studies of PL as a function of atmosphere type (oxidative or reductive), annealing temperature, number of defects, size of crystallites and the excitation energy ($E_{ex} \geq E_b$ or $E_{ex} < E_b$) have allowed two bands to be distinguished in visible PL [27, 28]. "Green" band with the center at 530 – 510 nm is preferably attributed to radiative recombination at shallow electron-trapping sites such as $V_{O^{2-}}$ oxygen vacancies, while shallowly trapped electrons recombine with holes from the valent band (VB). "Red" band centered around 600 – 690 nm is attributed to recombination at deeper electron traps V_{O^-}/Ti^{3+}, V_O/Ti^{3+} [27, 28]. It has been established that "Red" band of photoluminescence (PL) is also observed at the excitation energies higher and lower than the band gap of TiO_2; and the PL mechanisms have been suggested for defect-containing anatase [27].

PL studies of brookite are scarce, addressing only single-phase brookite samples which were obtained by hydrothermal synthesis, and these studies were conducted for the excitation energies ranging close to the energy gap width [10, 11, 29]. An earlier study has provided data only on the visible PL recorded in the range of 400 to 650 nm for aggregated nanocrtystalline brookite powders [29]. Later on, PL spectra taken from the hydrothermally synthesized nanocrystallites of brookite, which have a good crystallinity quality and a low aggregation degree, showed not only a weak visible PL but also an intense photoluminescence in the near-IR (NIR) region in the vicinity of 860 nm similar to NIR PL in rutile [10, 11]. It has been established that in brookite it is NIR-PL that is caused by radiative recombination between deeply trapped electrons and valence band holes. The life time of such NIR PL in brookite (or the lifetime of deeply trapped electrons) is several times longer than the lifetime of the visible PL and shallowly trapped electrons in anatase [10, 11]. In turn, similarly to the visible PL in anatase, the visible PL in brookite is assigned to radiative recombination between shallowly (or slightly deeper) trapped electrons and holes. Poorer crystallinity quality and the aggregation of brookite nanocrystallites result in a decrease in the NIR-PL and in enhanced visible PL. Similarly to the NIR PL in rutile and visible PL in anatase, the NIR and visible PL in brookite react differently on the type of the environment, including oxygen atmosphere. No final conclusion has yet been made on the type of lattice intrinsic defects responsible for NIR PL in titanium dioxides, however, the majority of researchers do not assign NIR PL to radiative recombination at the defect sites like oxygen vacancies [25, 30].

Unlike the well-studied mixed anatase/rutile matrices, photoluminescence research of anatase/brookite titanium dioxide is close to non-existent; however, there are preliminary photoluminescence data available on aggregated nanocrystalline powder synthesized using the wet precipitation method [31]. In the visible PL part of the spectrum, a broad band characteristic of anatase and brookite is observed. NIR band was also observed, which is supposed to be attributed to radiative recombination at deep traps in brookite.

The purpose of this study is to elucidate the properties of NIR-PL for the precipitated powders having nanocrystalline anatase/brookite structure. To this end, the effect of annealing in oxygen atmosphere on NIR PL was studied, the crystallinity quality of brookite phase and its content in the powder were analyzed, and the NIR PL was also investigated as a function of excitation energy. The structural state and composition of anatase/brookite samples were characterized with XRD, Raman spectroscopy, IR-spectroscopy, scanning and transmission electron microscopy. The energies of band gap and absorption properties were estimated by diffuse reflectance. It was found that NIR-PL observed in anatase/brookite aggregated powders demonstrate the behavior typical of NIR PL in brookite. Unlike the visible luminescence, NIR luminescence centered at 865-870 nm did not decrease under annealing in oxygen, as the content of oxygen vacancies decreases and quality of crystallinity improves. On the contrary, NIR PL increases. NIR PL also grows with increasing brookite content in the powder up to 30 %, which is indicative of the absence of NIR PL quenching effect in bi-phase anatase/brookite matrices. NIR-PL is observed for the excitation energy equal or less than the band gap width and demonstrates sublinear growth with excitation power. Possible mechanism is discussed for NIR-PL emission in brookite at visible excitation.

The obtained results provide evidence that the bi-phase powders prepared by wet precipitation route have intrinsic defects in the brookite lattice, which act as deep electron traps that may favor photocatalytic redox reactions.

2. Experimental part

TiO_2 powders with anatase/brookite structure were prepared by wet precipitation technique, and details of TiO_2 preparation can be found in Ref. [14]. In brief, a certain amount of titanium (IV) n-butoxide was added into the pure deionized water. To fabricate brookite-rich nanocrystalline powders, the samples were heated up to the boiling point under continuous stirring and aged at this temperature for 4 h. To remove the remaining organic species, the powders were centrifuged, redispersed twice in ethanol or water, and then dried in air at 120 °C for 3 h. Brookite-poor powders were prepared by the same hydrolysis route but without aging stage at boiling point. All powders were further annealed in oxygen atmosphere at 400 and 550 °C for 2 hours in TG-92 chamber. Oxygen pressure was 1 atm. and oxygen flow rate was 15 ml/min. To avoid the formation of high-temperature rutile phase in the samples, the maximum annealing temperature was limited to no more than 550 °C.

X-ray diffraction (XRD), Raman micro-spectroscopy, high resolution transmission electron microscopy (HRTEM) and electron diffraction were employed to characterize structural properties, defects and crystallinity quality of TiO_2 nanopowders. The XRD patterns of samples were recorded by Shimadzu MAXima-X XRD-7000 (Shimadzu, Japan) automatic diffractometer with CuKα radiation ($\lambda = 1.5406$ Å) in 2θ angle range 10 – 80 ° with a step 0.03 ° and an exposure time of 10 sec at each step. The volume fractions and structural characteristics of constituent phases were calculated employing PCW 2.4 software (http://powdercell-forwindows.software.informer.com/2.4). High resolution TEM images and electron diffraction patterns were obtained with the help of JEM-2100 and JEM-200CX microscopes (JEOL, Japan). The specific surface area of the powder was determined with the Brunauer–Emmett–Teller model (BET method) using Gemini VII 2390 microcrystal analyzer. Raman and photoluminescence spectra were excited by a low-power (up to 3 mW) laser irradiation at wave length of 405 and 532 nm at room temperature, and they were recorded by a Renishaw inVia Reflex laser Raman spectrometer (Renishaw, UK), providing a focal spot on the samples of 1 – 2 μm diameter. Spectral resolution was about 0.5 cm^{-1}. The acquisition time was up to 10 s, and each spectrum was scanned 3 times. Several spectra were taken for each sample to test for homogeneity and reproducibility. Raman and photoluminescence spectra were analyzed with multi-peak Gaussian fitting method using the "Peakfit v 4.11" software package. Infrared spectroscopy was used to identify the remaining hydrocarbon species and hydroxyl groups on the surface of TiO_2 powder particles. The infrared spectra of samples were registered on Vertex 80 IR Fourier spectrometer (Bruker, Germany) using MVP-Pro ATR Accessory with diamond crystal (Harrick, USA) in the interval of 4000 – 400 cm^{-1}.

Optical absorption properties and band gap were evaluated with diffuse reflectance spectroscopy. The diffuse reflectance spectra of the powders were measured with a Shimadzu UV-3600 spectrophotometer (Japan) using $BaSO_4$ as a reference. The reflectance data was converted to the extinction coefficient $F(R_\infty)$ values according to the Kubelka–Munk equation:

$$F(R_\infty) = \frac{(1 - R_\infty)^2}{2R_\infty}, \tag{1}$$

where $F(R_\infty)$ is proportional to the extinction coefficient. The transformed Kubelka–Munk function was constructed by plotting $(F(R_\infty) \cdot h\nu)^{1/2}$ against the energy of excitation source to obtain the band gap of TiO_2 powder, which is considered to be an indirect band-gap semiconductor [32].

3. Results and discussion

3.1. Structural and photoluminescence properties of the precipitated TiO_2 powder with nanocrystalline anatase/brookite matrix

TiO_2 powders synthesized via the wet precipitation route with the thermal aging of hydrolysis products [14, 16] demoinstrate XRD and Raman spectra which show that the powder is bi-phase anatase/brookite with nanocrystalline structure (Fig. 1(a,b)). The indexing of XRD reflections and curve-fitting of XRD patterns were carried out using a bi-phase model: the orthorhombic structure of brookite (S. G. Pcab, JCPDS no. 029-1360) and the tetragonal structure of anatase (S. G. I4(1)/amd, JCPDS no. 21-1272). According to the profile-fitting of XRD spectra, the brookite phase content is up to 33 %, and the average crystallite size is 7.5 – 8 nm for both phases. Table 1 gives the structural characteristics determined using profile-fitting of the XRD spectra. HRTEM study of these powders reveals a minor amount of amorphous phase, no more than 5 % [16], and the average crystallite size of about 6.5 (± 0.5) nm (Fig. 1(c)). SEM images demonstrate a high aggregation in the powders (Fig. 1(d)).

Figure 2 displays a typical PL spectrum with excitation energy of 532 nm taken for the powder with the anatase/brookite matrix containing 33 % of brookite. The spectrum demonstrates a wide band of visible light and NIR PL emission. Visible PL emission can be described with three most intensive Gaussian sub-bands centered at 591 nm (2.1 nm), 638 nm (1.95 nm), and 693 nm (1.8 eV). The observed visible PL emission with below-bandgap excitation of 2.33 eV (green excitation) means that a great number of defects are presented in the anatase phase, which act as deep electron traps and as radiative recombination centers [28]. All the three bands of visible emission can be assigned to radiative recombination on the surface defects such as oxygen vacancies, Ti^{3+} defects and hydroxyl groups which all are the predominant trapping sites for low-temperature sol-gel nano-powders [20]. Decomposition of the spectrum shows the presence of sub-bands

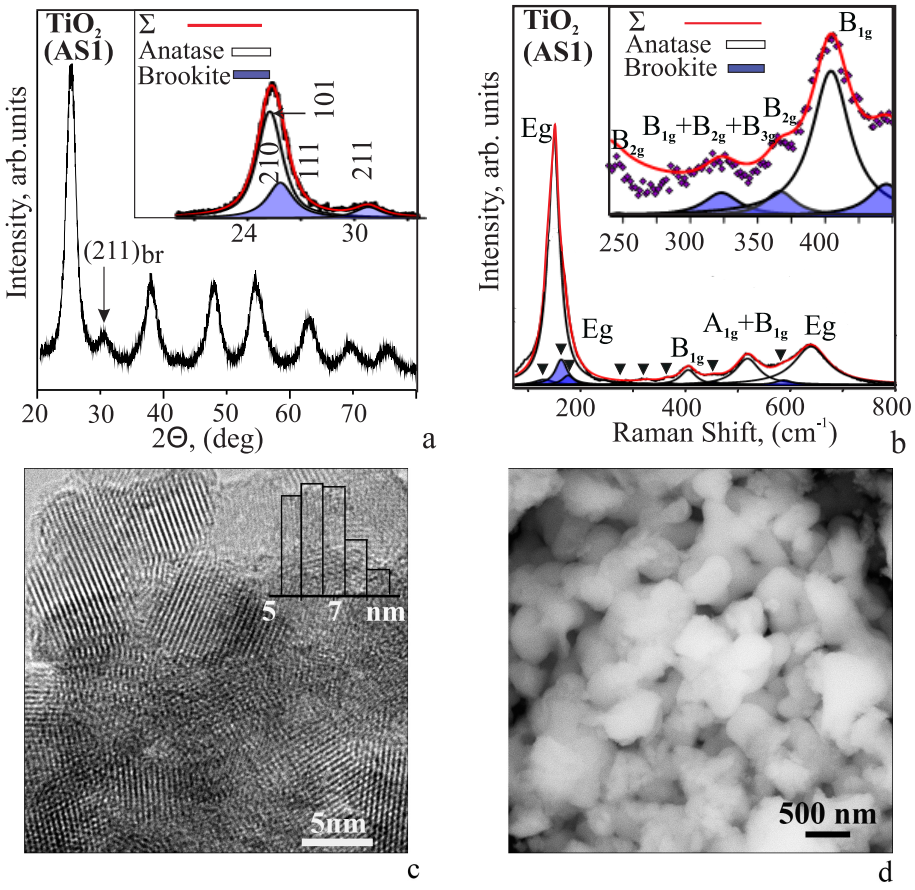

FIG. 1. Structure of precipitated TiO_2 powder (AS1) with nanocrystalline rich-brookite matrix: a – XRD pattern (XRD spectrum and profile calculated with a two-phase model are shown in the insert); b – Raman spectrum, brookite modes are marked by triangles, excitation is 532 nm; c,d – HRTEM and SEM images, respectively. Crystallite size distribution is shown in the insert.

characteristic of the visible PL observed in the conditions of green excitations for the anatase phase containing an appreciable number of oxygen vacancies [28]. Thus, visible emission at 1.95 and 1.8 eV can be attributed to the deexcitation from the deep levels of oxygen vacancies associated with Ti^{3+} in anatase lattice to the ground state [20, 21, 28]. In turn, the sub-band at 2.1 eV is due to the deexcitation from lower levels in Ti^{3+} 3d states of TiO_2 lattice to the deep levels created by OH^- group [20]. The presence of OH^- hydroxyl groups is supported with the observed wide band at 2500 – 3700 cm^{-1} and the vibrational mode at 1633 cm^{-1} in the IR-spectra of the powders. Besides, it should be considered that the surface oxygen vacancies of the aggregated brookite nanoparticles are also deemed responsible for the visible PL observed.

One Gaussian sub-band at 870 nm (1.42 eV) is located in the near-IR region of the spectrum. This NIR PL emission at 1.42 eV could be a signature of the brookite phase and could be associated with the deep traps at the brookite lattice defects. Further, in order to clarify the properties of the observed NIR PL and the defect states responsible for this PL, a comparative study was carried out for visible and NIR PL, and also for the light absorption and structural properties of bi-phase nano-powders depending on annealing in oxygen. NIR PL was estimated for the powders with different brookite contents. NIR PL was studied as a function of excitation energy.

3.2. Structural, photoluminescence and light absorption properties of TiO_2 powder with nanocrystalline anatase/brookite matrix: effect of annealing in oxygen atmosphere and brookite content

Under annealing in oxygen at temperatures of 400 and 550 °C, the bi-phase structure of brookite-rich powders (AS1) remains (Fig. 3(a)), however, according to the results of profile-fitting of XRD spectra, the brookite fraction falls from 33 down to 17 % at a temperature of 550 °C (Table 1). The electron diffraction study shows that there is no high-temperature rutile phase, with up to ten SAED (selected area electron diffraction) patterns obtained from various parts of the powder (Fig. 3(b)). For brookite-rich sample, with increasing annealing temperature, anatase and brookite crystallite size consequently grows, and amounts to 10 and 12.5 nm, respectively, at the annealing temperature of 400 °C, and 15 and 17 nm at the annealing temperature of 550 °C. Evaluated using the BET method, the specific surface area decreases from 245 m^2/g (AS1) down to 140 m^2/g (AS1 + 440 °C) and to 115 m^2/g (AS1 + 550 °C). Microstrains, which are indicative

TABLE 1. Structural characteristics determined using profile-fitting of XRD spectra for as-prepared (AS1) and annealed nanopowders

Structural properties *		TiO_2 bulk	TiO_2 (AS1)	TiO_2 (AS1) +400O_2 °C	TiO_2 (AS1) +550O_2 °C
Phase composition, brookite/anatase(%)			33 /67	31/ 69	17 / 83
	Anatase				
Crystalllite size, nm			7.5(±0.4)	10(±0.5)	15(±0.8)
Lattice parameters, nm	a	3.785	3.804(3)	3.796(3)	3.786(3)
	b	9.514	9.458(7)	9.481(7)	9.511(7)
Unit cell volume		136.3	136.8(3)	136.6(3)	136.3(3)
Microstrains, %			0.6	0.6	0.1
	Brookite				
Cristallite size, nm			8.0 (±0.4)	12(±0.5)	17(±0.8)
Lattice parameters, nm	a	5.135	5.207(4)	5.211(4)	5.151(4)
	b	9.166	9.066(7)	9.066(7)	9.127(7)
	c	5.436	5.355(4)	5.384(4)	5.443(4)
Unit cell volume		255.8	252.8(6)	254.4(6)	255.9(6)
Microstrains, %			0.6	0.4	0.2

*The typical values of R factors: $R_p = 7 \div 9$ and $R_{wp} = 9 \div 11$.

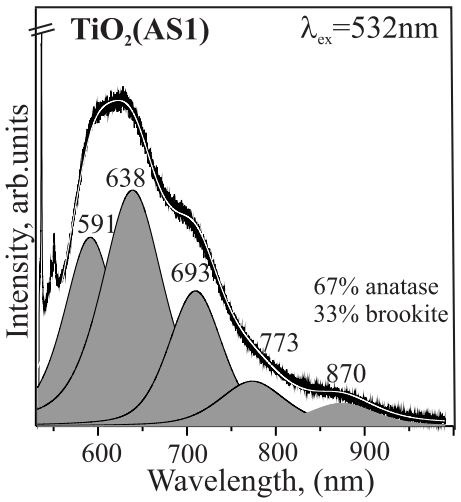

FIG. 2. PL spectrum for anatase/brookite nanopowder with high content of brookite phase

of defect concentration, decrease consistently from 0.63 down to 0.6 % (400 °C) and 0.1 % (550 °C) for anatase; and from 0.6 down to 0.4 % (400 °C) and 0.2 % (550 °C) for brookite. The unit cell volume decreases for anatase and grows for brookite, approaching the bulk values. For the annealed brookite, the deviation of the unit cell from the bulk value is insignificant: 0.5% at an annealing temperature of 400 °C and 0.2 % at 550 °C (Table 1).

Being sensitive to nanocrystallite size, to defect concentration and to crystallinity quality, the Raman spectra undergo substantial changes (Fig. 3(c)) as the annealing temperature grows.

Figures 3(c) (insert), 3(d) and Table 2 demonstrate the results of spectra decomposition, which was carried out using the Gaussian-Lorentzian profile of Raman bands. The spectra decomposition reveals all six Raman peaks of anatase ($3E_g$, A_{1g} and $2B_{1g}$) and the majority of vibrational modes of brookite having very strong, strong and medium intensities according to the notations reported by Iliev M. et al [33]. As the annealing temperature grows, all the anatase peaks demonstrate an increase in intensity and the peak narrowing (i.e., decreasing FWHM) and the red-shift of peak positions.

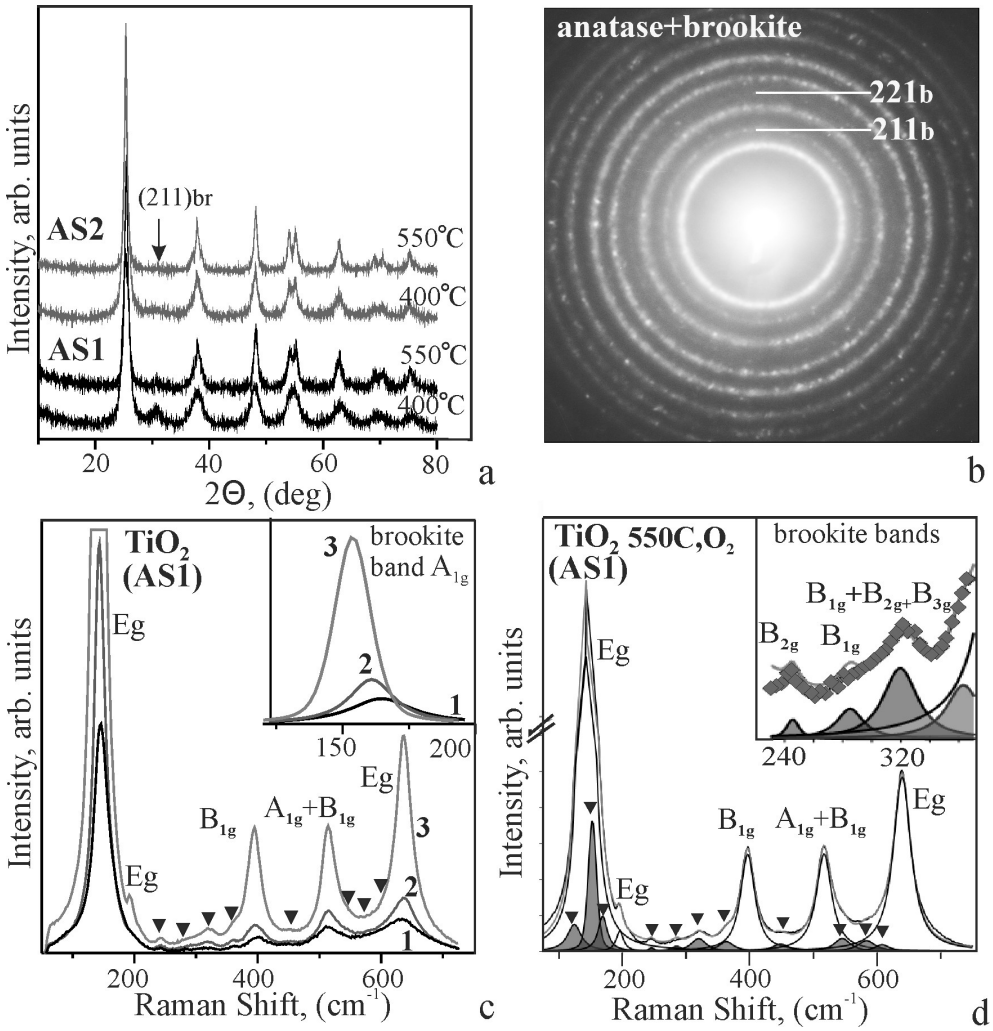

FIG. 3. XRD (a), electron diffraction (b) and Raman spectra (c,d) for anatase/brookite powders annealed in oxygen atmosphere, brookite modes are marked by triangles; excitation is 532 nm. AS1, AS2 – powders with rich- and poor-brookite composition, respectively. 1 – as-prepared powder; 2, 3 – powders annealed at 400 and 550 °C, respectively.

The same tendency is observed for all brookite peaks, including the spectra of powders annealed at 550 °C. As an example, Fig. 3(c) (insert) exhibits a brookite peak corresponding to the most intense vibrational mode A_{1g} for as-prepared and annealed powders. Despite the considerable decrease in brookite content at an annealing temperature of 550 °C, the intensity of Raman peak grows owing to the increased crystallinity quality and smaller number of defects in brookite structure. Besides, for powder annealed at 550 °C, Raman phonon wavenumbers (in cm^{-1}) for brookite and anatase components of the nanopowders are quite close to those for bulk crystalline brookite [33] and anatase [34], respectively (Table 2). For the powders annealed at 550 °C, the crystallite sizes of both phases are larger than 15 nm and, according to a number of research works [35–38], the Raman peak shifts due to the size-induced phonon confinement effect should not be observed. Then the shifts of the Raman peak position, which are related to the structural disorder and defects (including interstitial atoms, vacancies and Vo/Ti^{3+} centers), should be very insignificant for these samples. Therefore, the results of XRD and Raman spectroscopy imply that, in the samples annealed at 550 °C, brookite as well as anatase particles exhibit good crystallinity quality and have relatively low defect concentration.

Figure 4(a) exhibits the PL spectra of brookite-rich (AS1) nanocrystalline powders as-prepared and annealed in oxygen atmosphere. It can be seen that all sub-bands of visible red PL, including those associated with deexcitation of oxygen-vacancy states, decrease appreciably at an annealing temperature of 400 °C already, the intensity maximum of visible PL being shifted to the short-wave region. At an annealing temperature of 550 °C, the visible PL intensity is observed to be close or slightly lower than the visible PL intensity at 400 °C. That may be caused by the growing content of anatase component, which makes the major contribution into the visible PL. The observed annealing behavior of visible PL confirms once again that this PL is mostly associated with recombination at the defect states. No signs of size factor influence on PL was found, which appears because of the quantum confinement effect in semiconductor nm-sized system. In this case, as the crystallite size grows from 7.5 up to 15 nm, which occurs at annealing, the PL maximum

TABLE 2. Peaks position and FWHM of vibration modes in Raman spectra of brookite-rich nanopowders, as prepared and annealed in oxygen atmosphere

Raman mode	Peak position / FWHM (in cm^{-1})				
	as prepared	annealing at 400 ° C, oxygen atm.	annealing at 550 ° C, oxygen atm.	Anatase mode, [34]	Brookite mode, [33]
(A_{1g}) **B***	130.5 / 42.8	125.7 / 35.2	124.4 / 26.3		**125** (m)
(E_g) **A***	149.3 / 26.5	147.1 / 19.8	143.1 / 13.7	**144** (vs)	
(A_{1g}) **B**	163.4 / 27.4	159.7 / 19.5	152.8 / 15.5		**152** (vs)
($B_{1g} + B_{2g}$) **B**	175.3 / 26.5	170.7 / 22.4	169.1 / 17.3		**169** (m), **160** (s)
(E_g) **A**	197.4 / 30.6	197.6 / 16.8	195.9 /13.7	**197** (w)	
(A_{1g}) **B**		247.1 / 8.1	245.6 / 11		**246** (s)
(B_{1g}) **B**		292.7 / 25.3	285.1 / 22.3		**283** (s)
($B_{1g}+B_{2g}+B_{3g}$) **B**	323.7 / 33.1	321.2 / 30.7	319.6 / 28.4		**327** (m), **325** (m), **318** (s)
(B_{2g}) **B**	365.5 / 36.1	363.8 / 28.3	363.1 / 28.3		**366** (s)
(B_{1g}) **A**	404.9 / 35.7	400.7 / 32.9	396.5 / 26.8	**399** (m)	
(B_{1g}) **B**	452.3 / 31.9	449.8 / 42.9	448.5 / 32.8		**449** (m)
($A_{1g} + B_{1g}$) **A**	517.7 / 54.6	519.1 / 42.9	516.3 / 29.2	**513, 519** (m)	
(A_{1g}) **B**			544.8 / 30.3		**545** (s)
(B_{2g}) **B**	586.5 / 38.6	586.5 / 34.1	583.0 / 32.9		**584** (m)
(E_g) **A**, (A_{1g}) **B**	641.3 / 79	640.9 / 52.7	638.9 / 33.4	**639** (m)	**640** (s)

* **B** – brookite, **A** – anatase

should be noticeably shifted to the long-wave region [35]. Annealing atmosphere plays a decisive role in decreasing the luminescence associated with oxygen vacancies. Annealing carried out in air at 400 °C leads even to some growth of the visible PL, which may be attributed to the improved crystallinity in the near-surface layers and to crystallization of the residual amorphous phase with annealing. HRTEM images confirm the lack of amorphous components in the powders.

In nanopowders of titanium dioxide under annealing in oxygen at 400 – 550 °C, the decrease in the content of oxygen vacancies agrees with the data available in literature [39]. For the studied nanocrystalline powders, this effect is confirmed with the comparative study of optical absorption properties of as-prepared and annealed powders, which was carried out using the diffuse reflectance method. Fig. 5 displays the transformed Kubelka–Munk function $(F(R) \cdot h\nu)^{1/2}$ vs. the energy of excitation for these samples, since TiO_2 would usually be considered as indirect band-gap semiconductor. In the range of 3 to 2 eV (from 415 to 620 nm), absorption falls for the powders annealed in oxygen as compared to the as-prepared powder. This fact definitely supports the decrease in the concentration of deeper trap states associated with the oxygen vacancies [30] and agrees well with the observed decrease in the PL in the red region over 500 nm. In the range greater than 3 eV, on the contrary, absorption is greater for the annealed powders, which can be mostly due to the self-trapped states and size quantization effect [40].

To estimate the bandgap width for indirect band-gap semiconductors, the following dependence of absorption coefficient (K) on radiation energy should be used:

$$K = \begin{cases} 0, & h\nu < E_G - E_P; \quad (2a) \\ A\left(h\nu - E_G + E_P\right)^2, & E_G + E_P > h\nu > E_G - E_P; \quad (2b) \\ A\left(h\nu - E_G + E_P\right)^2 + B(h\nu - E_G - E_P)^2, & h\nu > E_G + E_P, \quad (2c) \end{cases}$$

where $h\nu$ is the excitation energy, E_G is the band gap, E_P is the value of the phonon energy associated with the indirect transition, $\sqrt{K}$ is proportional to $\alpha \cdot h\nu$ (α is the extinction coefficient) [41] and, therefore, is also proportional to $(F(R_\infty) \cdot h\nu)$. Based on this equation, we would expect to observe two linear regions in the plot of the square root of the absorption coefficient: the first linear region (eq. (2b)) being associated with phonon absorption, and the second linear region (eq. (2c)) being associated with phonon emission. However, only one linear region is presented in the plot

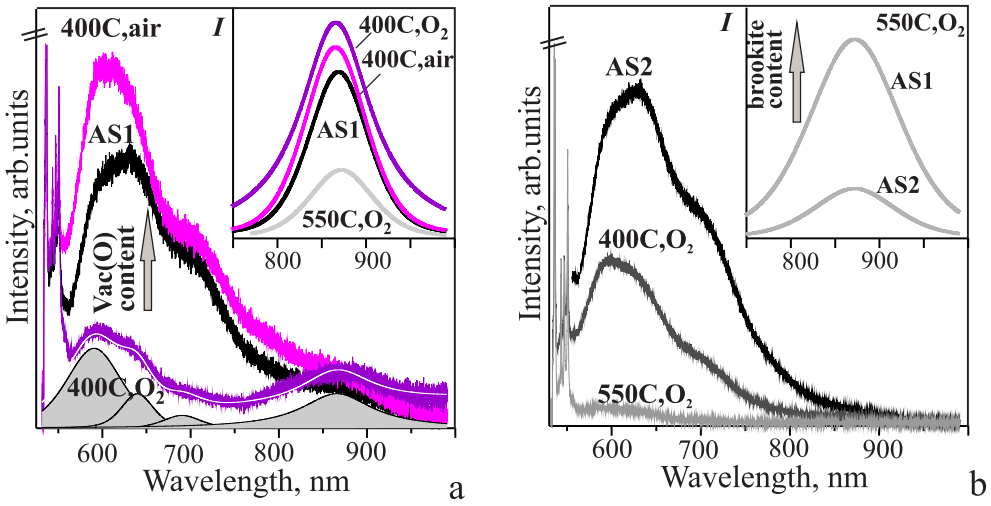

FIG. 4. PL spectra for brookite-rich (AS1) (a) and brookite-poor (AS2) nanopowders annealed at 400 and 550 °C in oxygen atmosphere and in air (the annealing parameters are given at the corresponding curves). In the inserts, intensity of NIR PL sub-band is given for different annealing temperatures (a) and brookite content (b). The laser excitation is 532 nm.

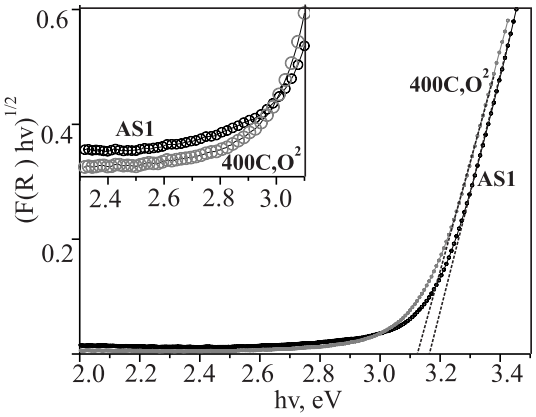

FIG. 5. Transformed Kubelka–Munk function $(F(R) \cdot h\nu)^{1/2}$ vs. excitation energy ($h\nu$) for brookite-rich nanopowders: as-prepared (AS1) and annealed in oxygen atmosphere at 400 °C

$(F(R) \cdot h\nu)^{1/2}$ vs. excitation energy (Fig. 5). In this case, because the phonon emission region is masked, only the value of $(E_G + E_P)$ can be determined [42]. Hence, the band gap of TiO_2 (AS1) and annealed TiO_2 (AS1) nanopowders are suggested to be slightly less than 3.18 and 3.16, respectively.

The decrease in the content of oxygen vacancies with annealing at 400 °C appears to be not that significant, as no widening of the band gap width is observed. A slight decrease of the band gap (or red-shift) from 3.18 to 3.16 takes place with annealing at 400 °C and with the growth of crystallite size in TiO_2 nanopowders, and hence, the quantum size effects are prevalent. As follows from the literature data [40], for anatase nanoparticles the widening of the band gap width with decreasing crystallite size due to the quantum size effect, should be observed exactly for the crystallite crystallite size less than 17 nm.

For brookite-rich nanopowder, annealing behavior of NIR PL demonstrates a fundamental difference from the behavior of visible PL. Fug. 4(a) (insert) exhibits the NIR PL sub-band resulted from decomposition of PL spectra. As can be seen, the annealing in oxygen at 400 °C and the decrease in the content of traps associated with oxygen vacancies in dioxide titanium phase results even in the growth of NIR PL rather than in a decrease. Besides, a somewhat lower growth in the intensity of NIR PL sub-band is also observed under annealing in air at 400 °C. For anatase/brookite matrix, the observed behavior of NIR PL sub-band allows one to assign the luminescence to the deep defect levels in brookite. As established earlier, NIR PL is enhanced in brookite as the crystallinity quality improves [11], and it is expected to be growing similarly to the case of rutile [25] in oxygen atmosphere as the content of oxygen vacancies decreases.

At the same time, annealing at 550 °C is accompanied with the decrease in the intensity of NIR PL sub-band, although according to the XRD and Raman spectroscopy data the brookite phase exhibits good crystallinity quality and has relatively low defect concentration (Fig. 4(a), insert). The nearly two-fold decrease in the content of brookite (from

33 to 17 %) may be the major reason for the decrease in NIR intensity, because no effect of quenching of NIR PL was observed in the mixed bi-phase anatase/brookite samples, although NIR PL quenching of rutile does occur in bi-phase anatase/rutile matrices [24]. The above discussed suggestion is confirmed with the comparative study carried out on photoluminescence of TiO_2 (AS2) samples containing no more than 3 % of brookite, which were obtained without the thermal aging stage (Fig. 3(a)). The as-prepared samples synthesized following this technique are found to be X-ray amorphous [16]; and the annealing at 400 and 550 °C in oxygen leads to the formation of nanocrystalline brookite-poor structure. For the brookite-poor powder annealed at 550 °C, the crystallite sizes and the Raman phonon wavenumbers (in cm^{-1}) for brookite and anatase components are practically the same as those for the brookite-rich powder annealed at 550 °C. For the brookite-poor samples, similarly to the brookite-rich nanopowders, annealing in oxygen also results in the considerable decrease in visible PL (Fig. 4(b)). In addition, intensity of NIR PL in these brookite-poor samples is significantly lower than that in brookite-rich samples (Fig. 4(b), insert). Therefore, it can be deduced that, quenching of NIR PL is not essential in mixed anatase/brookite nanopowders with brookite content up to 20 – 30 %.

As demonstrated by the experiments carried out with annealing in oxygen, NIR PL of anatase/brookite aggregated powders exhibit a behavior characteristic of NIR PL in brookite. However, it turns out quite significant that NIR PL is observed as well as the visible PL at excitation energy less than band-gap energy for these powders. Further, a discussion of possible PL mechanism is provided and the PL spectra are considered for the energy excitation close to the value of band gap energy.

3.3. NIR photoluminescence in anatase/brookite nanopowders at violet and green excitation

Figure 6 exhibits a PL spectrum recorded at the excitation energy of 405 nm ($E_{ex} \approx E_b$), for the brookite-rich nanopowder annealed at 400 °C in oxygen. In these samples, the maximum content of brookite and the crystallinity quality are greater than those of as-prepared nanopowders. The spectrum, along with the visible band, demonstrates an intense NIR PL, and the comparison with NIR PL recorded for the excitation energy of 532 nm ($E_{ex} < E_b$) does not reveal any appreciable shift of the maximum of luminescence band. It means that in the both cases the NIR PL is associated with radiative recombination at the same deep defect levels in brookite. Intensity of NIR band grows with the excitation power considerably more than that of visible PL but it follows the sublinear law $I \sim P^{\gamma}$ ($\gamma = 0.7$), indicating the saturation of these levels at high excitation energy [22].

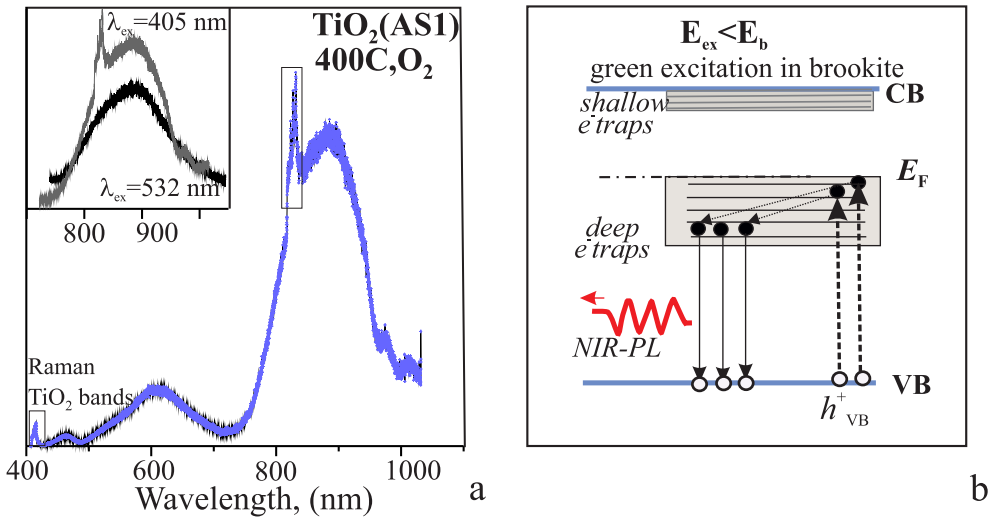

FIG. 6. a – PL spectrum of brookite-rich nanopowder at laser excitation of 405 nm. In insert, NIR band for different laser excitations, power $P = 0.3$ mW. Raman band are marked with rectangles. b – Scheme of possible NIR PL mechanism in brookite at sub-bandgap excitation.

According to the reports on the investigation of photoluminescent behavior in brookite [11], NIR emission observed at UV-excitation ($E_{ex} > E_b$ or $E_{ex} \approx E_b$) is assigned to radiative recombination between deeply trapped electrons and valence band holes, with intrinsic defects acting as deep traps of photogenerated electrons excited from the valence band. Then, NIR PL observed at green excitation with $E_{ex} < E_b$ can be caused by the sub-bandgap (below-bandgap) excitation of electrons from the valence band to reach some defect states, their migration into these deep traps and, finally, their radiative recombination with the valence band holes. Fig. 6(b) displays a schematic illustration of this NIR PL mechanism in brookite. A similar mechanism has earlier been suggested for the red PL in anatase at visible (blue, green and yellow) excitation [27, 28], and it is considered possible as for the red PL as for the NIR PL in brookite at visible excitation. The suggested NIR PL mechanism is supported with the data of transient absorption (TA) spectroscopy of TiO_2 brookite nanocrystals [10, 11]. Three groups of surviving electrons were found for brookite using TA spectroscopy.

Apart from the largest group of the deeply trapped electrons, there are also a number of groups of surviving electrons at excitation in brookite: these are small groups, where the first group includes free and shallow-trapped electrons and the second group includes trapped electrons. Both of the groups may be assigned to various oxygen vacancies. It is the electron traps associated with the second group that can act as intermediate states, and the sub-bandgap (green) excitation can promote electrons to these defect states from the VB. Within the framework of the suggested mechanism, the decrease in the concentration of oxygen vacancies of the second group, which is clearly observed at annealing in oxygen, may be the reason for the lower intensity of NIR PL emission at visible excitation in the annealed samples.

4. Conclusions

NIR-PL properties were studied for the precipitated TiO_2 nanopowders having anatase/brookite structure, i.e., the effect caused on photoluminescence by annealing at 550 °C in oxygen, by crystallinity quality and defect concentration and by the content of brookite phase. The dependence of NIR PL on excitation energy ($E_{ex} \approx E_b$ and $E_{ex} < E_b$) was also considered. The structural properties of the powders were characterized by XRD, HRTEM, SEM, electron diffraction and Raman spectroscopy. Optical absorption properties and band gap were evaluated using the diffuse reflectance method.

It was found that NIR PL in brookite-rich powders (up to 33 %) show the signs of NIR PL of brookite, which is associated with the lattice intrinsic defects of brookite, acting as deep electron traps. Unlike the visible PL, the intensity of NIR PL emission in bi-phase powders grows at annealing in oxygen, while the content of oxygen vacancies decreases and the structural disorder of brookite crystal lattice decreases (crystallinity quality of brookite improves). With the brookite content growth, NIR PL grows as well, which is indicative of the insignificant NIR PL quenching effect in bi-phase anatase/brookite nanopowders.

NIR PL is also observed for the band ($E_{ex} \approx E_b$) and below-bandgap ($E_{ex} < E_b$, green) excitation. The NIR PL mechanism at below-bandgap excitation is assumed to be similar to the mechanism for the red PL at sub-band excitation of nanocrystalline anatase, which has earlier been suggested by Pallotti et al. [27]. At below-bandgap excitation of brookite, the electrons excited from the valence band can get into some intermediate states associated with defects and then migrate to deep traps and escape these traps by way of NIR radiative recombination with the valence band holes.

The obtained results provide evidence that in the precipitated nanopowders with anatase/brookite structure, brookite contains deep defect traps, which are considered to be favorable for photocatalytic redox reactions, with the deep level lattice defects acting as electron traps for band ($E_{ex} \approx E_b$) as well as for sub-bandgap green ($E_{ex} < E_b$) excitation(s).

References

[1] Katal R., Masudy-Panah S., et al. A review on the synthesis of the various types of anatase TiO_2 facets and their applications for photocatalysis. *Chemical Engin. J.*, 2020, **384**, 123384.

[2] Verma R., Gangwar J., Srivastava A.K. Multiphase TiO_2 nanostructures: a review of efficient synthesis, growth mechanism, probing capability, and applications in bio-safety and health. *RSC Advances*, 2017, **7**, P. 44199–44224.

[3] Miyoshi A., Nishioka S., Maeda K. Water splitting on rutile TiO_2-based photocatalysts. *Chemistry: A European J.*, 2018, **24**, P. 1–17.

[4] Paolo A. Di, Bellardita M., Palmisano L. Brookite, the least known TiO_2 photocatalyst. *Catalysts*, 2013, **3**, P. 36–73.

[5] Monai M., Montini T., Fornasiero P. Brookite: nothing new under the sun. *Catalysts*, 2017, **7**, P. 304–323.

[6] Choi M., Yong K. A facile strategy to fabricate high-quality single crystalline brookite TiO_2 nanoarrays and their photoelectrochemical properties. *Nanoscale*, 2014, **6**, P. 3900–13909.

[7] Li Z., Cong S., Xu Y. Brookite vs anatase TiO_2 in the photocatalytic activity for organic degradation in water. *ACS Catalysis*, 2014, **4**, P. 3273–3280.

[8] Ohno T., Higo T., et al. Dependence of photocatalytic activity on aspect ratio of brookite TiO_2 nanorod and drastic improvement in visible light responsibility of a brookite TiO_2 nanorod by site-selective modification of Fe3+ on exposed faces. *J. of Molecular Catalysis A: Chemical*, 2015, **396**, P. 261–267.

[9] Mamakhel A., Yu J., et al. Facil synthesis of brookite TiO_2 nanoparticles. *Chem. Commun.*, 2020, **56**, P. 15084–15087.

[10] Vequizo J.M., Matsunaga H., et al. Trapping-induced enhancement of photocatalytic activity on brookite TiO_2 powders: comparison with anatase and rutile TiO_2 powders. *ACS Catalysis*, 2017, **7**, P. 2644–2651.

[11] Vequizo J.M., Kamimura S., Ohno T., Yamakata A. Oxygen induced enhancement of NIR emission in brookite TiO_2 powders: comparison with rutile and anatase powders. *Phys. Chem. Chem. Phys.*, 2018, **20**, P. 3241–3248.

[12] Zhao H., Liu L., Andino J.M., Li Y. Bicrystalline TiO_2 with controllable anatase-brookite phase content for enhanced CO_2 photoreduction to fuels. *J. of Materials Chemistry A*, 2013, **1**, P. 8209–8216.

[13] Fischer K., Gawel A., et al. Low-temperature synthesis of anatase/rutile/brookite TiO_2 nanoparticles on a polymer membrane for photocatalysis. *Catalysts*, 2017, **7**, P. 209–223.

[14] Kozhevnikova N.S., Ulyanova E.S., et al. Low-temperature sol-gel synthesis and photoactivity of nanocrystalline TiO_2 with the anatase/brookite structure and an amorphous component. *Kinetics and Catalysis*, 2019, **60**, P. 325–336.

[15] Vorokh A.S., Kozhevnikova N.S., et al. Facile, rapid and efficient doping of amorphous TiO_2 by pre-synthesized colloidal CdS quantum dots. *J. Alloys and Comp.*, 2017, **706**, P. 205–214.

[16] Ulyanova E.S., Zamyatin D.A., et al. Local environment of CdS nanoparticles incorporated into anatase/brookite matrix via sol-gel route: HRTEM, Raman spectroscopy and MD simulation. *Materials Today Communications*, 2020, **25**, 101465.

[17] Cong Y., Zhang J., Chen F., Anpo M. Synthesis and Characterization of nitrogen-doped TiO_2 nanophotocatalyst with high visible light activity. *J. Phys.Chem.*, 2007, **111**, P. 6976–6982.

[18] Yan J., Wu G., et al. Understanding the effect of surface/bulk defects on the photocatalytic activity of TiO_2: anatase versus ritule. *PCCP*, 2013, **15**, P. 10978–10988.

[19] Abazovic N.D., Comor M.I., et al. Photoluminescence of anatase and rutile TiO_2 particles. *J. Phys. Chem. B*, 2006, **110**, P. 25366–25370.

[20] Mathew S., Prasad A.K., et al. UV-Visible photoluminescence of TiO_2 nanoparticles prepared by hydrothermal method. *J. Pluoresc.*, 2012, **22**, P. 1593–1599.
[21] Chetibi L., Busko T., et al. Photoluminescence properties of TiO_2 nanofibers. *J. Nanopart. Res.*, 2017, **19**, 129.
[22] Zhang W.F., Zhang M.S., Yin Z., Chen Q. Photoluminescence in anatase titanium dioxide nanocrystals. *Appl. Phys. B*, 2000, **70**, P. 262–265.
[23] Preclikova J., Galar P., et al. Nanocrystalline titanium dioxide films: Influence of ambient conditions on surface- and volume-related photoluminescence. *J. of Appl. Phys.*, 2010, **108**, P. 113502.
[24] Knorr F.J., Mercado C.C., McHale J.L. Trap-state distributions and carrier transport in pure and mixed-phase TiO_2: influence of contacting solvent and interphasial electron transfer. *J. Phys. Chem. C*, 2008, **112**, P. 12786–12794.
[25] Shi J., Chen J., et al. Photoluminescence characteristics of TiO_2 and their relationship to the photoassisted reaction of water/methanol mixture. *J. Phys. Chem. C*, 2007, **111**, P. 693–699.
[26] Wang X., Feng Z., et al. Trap states and carrier dynamics of TiO_2 studied by photoluminescence spectroscopy under weak excitation conditio. *PCCP*, 2010, **12**, P. 7083–7090.
[27] Pallotti D.K., Passoni L., et al. Photoluminescence mechanisms in anatase and rutile TiO_2. *J. Phys. Chem. C*, 2017, **121**, P. 9011–9021.
[28] Mascaretti L., Russo V., et al. Excitation wavelength- and medium-dependent photoluminescence of reduced nanostructured TiO_2 films. *J. Phys. Chem. C*, 2019, **123**, P. 11292–11303.
[29] Bellardita M., Paolaa A., et al. Preparation and photoactivity of samarium loaded anatase, brookite and rutile catalysts. *Appl. Catalysis B: Environmental*, 2011, **104**, P. 291–299.
[30] Santara B., Giri P.K., Imakita K., Fujii M. Evidence for Ti interstitial induced extended visible absorption and near infrared photoluminescence from undoped TiO_2 nanoribbons: an in situ photoluminescence study. *J. Phys. Chem. C*, 2013, **117**, P. 23402–23411.
[31] Ulyanova E.S., Zamyatin D.A., Kolosov V.Yu., Shalaeva E.V. Visible light photoluminescence in TiO_2/CdS nanopowders synthesized by sol-gel route: effect of gel aging time. *Nanosystems: Phys. Chem. Math.*, 2020, **11**, P. 480–487.
[32] Lopez R., Gomez R. Band-gap energy estimation from diffuse reflectance measurements on sol-gel and commercial TiO_2: a comparative study. *J. Sol-gel Sci Technol.*, 2012, **61**, P. 1–7.
[33] Iliev M.N., Hadjiev V.G., Litvinchuk A.P. Raman and infrared spectra of brookite (TiO_2): Experiment and theory. *Vibrational spectroscopy*, 2013, **64**, P. 148–152.
[34] Ohsaka T., Izumi F., Fujiki Y. Raman Spectrum of Anatase, TiO. *J. of Raman Spectroscopy*, 1978, **7**, P. 321–324.
[35] Gupta S.K., Desai R., et al. Titanium dioxide synthesized using titanium chloride: size effect study using Raman spectroscopy and photoluminescence. *J. of Raman Spectroscopy*, 2010, **41**, P. 350–355.
[36] Sahoo S., Arora A.K., Sridharan V. Raman line shapes of optical phonons of different symmetries in anatase TiO_2 nanocrystals. *J. Phys. Chem. C*, 2009, **113**, P. 16927–16933.
[37] Georgescu D., Baia L., et al. Experimental assessment of the phonon confinement in TiO_2 anatase nanocrystallites by Raman spectroscopy. *J. of Raman Spectroscopy*, 2012, **43**, P. 876–883.
[38] Ceballos-Chuc M.C., Ramos-Castillo C.M., et al. The influence of brookite impurities on the Raman spectrum of TiO_2 anatase nanocrystals. *J. Phys. Chem. C*, 2018, **123**, P. 19921–19930.
[39] Ho Y.C., Hoque N.F., et al. Reduction of oxygen vacancy related traps in TiO_2 and the impacts on hybrid perovskite solar cells. *J. Phys. Chem. C*, 2017, **121**, P. 23939–23946.
[40] Lin H., Huang C.P., et al. Size dependency of nanocrystalline TiO_2 on its optical property and photocatalytic reactivity exemplified by 2-chlorophenol. *Appl. Catalysis B: Environmental*, 2006, **68**, P. 1–11.
[41] Moss T.S., Burrell G.J., Ellis B. *Semiconductor Opto-electronics*. Butterworths, London, 1973.
[42] Bost M.C. Mahan J.E. An investigation of the optical constants and band gap of chromium disilicide. *J. Appl. Phys.*, 1988, **63**, P. 839–844.

Submitted 31 January 2022; revised 23 June 2022; accepted 30 July 2022

Information about the authors:

Ekaterina S. Ulyanova – Institute of Solid State Chemistry of Ural Branch of the Russian Academy of Sciences, Pervomayskaya, 91, Ekaterinburg, 620990, Russia; ORCID 0000-0002-0922-3863; tsivileva.yekaterina@yandex.ru

Elizaveta V.Shalaeva – Institute of Solid State Chemistry of Ural Branch of the Russian Academy of Sciences, Pervomayskaya, 91, Ekaterinburg, 620990, Russia; ORCID 0000-0002-8617-3329; shalaeva@ihim.uran.ru

Yuriy S. Ponosov – M. N. Mikheev Institute of Metal Physics of Ural Branch of the Russian Academy of Sciences, S. Kovalevskaya, 18, Ekaterinburg, 620108, Russia; ORCID 0000-0001-5643-966X; ponosov@imp.uran.ru

Olga A. Lipina – Institute of Solid State Chemistry of Ural Branch of the Russian Academy of Sciences, Pervomayskaya, 91, Ekaterinburg, 620990, Russia; ORCID 0000-0003-3685-5337; LipinaOlgaA@yandex.ru

Alexey A. Markov – Institute of Solid State Chemistry of Ural Branch of the Russian Academy of Sciences, Pervomayskaya, 91, Ekaterinburg, 620990, Russia; ORCID 0000-0002-2454-8674; aamarkov1@yandex.ru

Conflict of interest: the authors declare no conflict of interest.